Using first-principles calculations to screen for fragile magnetism: Case study of $LaCrGe_3$ and $LaCrSb_3$

Manh Cuong Nguyen,[1,*] Valentin Taufour,[1,2] Sergey L. Bud'ko,[1,3] Paul C. Canfield,[1,3] Vladimir P. Antropov,[1] Cai-Zhuang Wang,[1] and Kai-Ming Ho[1,3]

[1]*Ames Laboratory – U.S. Department of Energy, Iowa State University, Ames, Iowa 50011, USA*
[2]*Department of Physics, University of California Davis, Davis, California 95616, USA*
[3]*Department of Physics and Astronomy, Iowa State University, Ames, Iowa 50011, USA*

(Received 19 November 2017; revised manuscript received 29 March 2018; published 2 May 2018)

In this paper, we present a coupled experimental/theoretical investigation of pressure effect on the ferromagnetism of $LaCrGe_3$ and $LaCrSb_3$ compounds. The magnetic, electronic, elastic, and mechanical properties of $LaCrGe_3$ and $LaCrSb_3$ at ambient condition are studied by first-principles density-functional theory calculations. The pressure dependences of the magnetic properties of $LaCrGe_3$ and $LaCrSb_3$ are also investigated. The ferromagnetism in $LaCrGe_3$ is rather fragile, with a ferro- to paramagnetic transition at a relatively small pressure (around 7 GPa from our calculations, and 2 GPa in experiments). The key parameter controlling the magnetic properties of $LaCrGe_3$ is found to be the proximity of the peak of Cr density of states to the Fermi level, a proximity that is strongly correlated with the distance between Cr atoms along the c axis, suggesting that there would be a simple way to suppress magnetism in systems with one-dimensional arrangement of magnetic atoms. By contrast, the ferromagnetism in $LaCrSb_3$ is not fragile. Our theoretical results are consistent with our experimental results and demonstrate the feasibility of using first-principles calculations to aid experimental explorations in screening for materials with fragile magnetism.

DOI: 10.1103/PhysRevB.97.184401

I. INTRODUCTION

Suppression of a ferromagnetic magnetic transition to zero temperature is of great interest as it may lead to quantum criticality where exotic phenomena such as non-Fermi liquid or unconventional superconductivity may emerge [1–7]. The common methods used to suppress magnetism in ferromagnetic materials includes doping or substituting magnetic element by other non- or very weak magnetic element or applying external pressure [1–5]. Doping or substitution always involves defects or randomness in the distributions of dopants and substituents, making it very difficult to investigate the effects of doping/substitution on the physical properties of materials in both experimental and theoretical studies. In addition, the choices of non- or very weak magnetic dopants or substituents that do not change the crystallography of the material can be very limited or even inexistent. In contrast, external pressure is a thermodynamic parameter which is considered cleaner and can be applied to any material. Recent examples in the family of Fe-based superconductors showed that the effect of pressure on magnetism can be very similar to the effect of chemical substitutions [8–12]. This makes external pressure a very promising controlling parameter to tune physical properties of materials. For practical reasons, small or intermediate pressures are more favorable than high and ultrahigh pressure, since high and ultrahigh pressure is difficult to handle by experiment, often are not hydrostatic and hard to model, and also can induce structural transformation. A theoretical screening tool to classify whether the magnetism in a material is fragile or not under pressure will be very helpful for efficient experiment explorations [4].

In this work, we demonstrate that first-principles calculations can be used as a tool to identify compounds with fragile magnetism by comparing two compounds $LaCrGe_3$ and $LaCrSb_3$ with different crystal structures (Fig. 1). $LaCrGe_3$ has a hexagonal crystal structure with $P6_3/mmc$ symmetry (space group No. 194) and $Z = 2$ formula units (f.u.) in the unit cell. $LaCrSb_3$ has an orthorhombic structure with $Pbcm$ symmetry (space group No. 57) and $Z = 4$ f.u. in the unit cell. Cr in both structures is coordinated by 6 Ge or Sb. Whereas the 6 coordinating Ge of Cr in $LaCrGe_3$ form a regular octahedron, the octahedron formed by 6 coordinating Sb of Cr in $LaCrSb_3$ is heavily distorted. The Cr–Sb bond is almost the same for 6 coordinating Sb, with less than 0.01 Å differences, but the Sb–Cr–Sb bonding angles are spread out largely from 80 to 130° with bond angle variance $\sigma^2 = 90.6$. Another difference between these two systems is in the dimensionality of the arrangement of Cr atoms. In $LaCrGe_3$, $CrGe_6$ octahedra form a one-dimensional line along lattice vector **c**. The $CrSb_6$ octahedra in $LaCrSb_3$ form wiggling planes perpendicular to lattice vector **a**.

At ambient conditions, $LaCrGe_3$ shows a ferromagnetic (FM) ground-state structure with magnetization aligned along the lattice vector **c**. $LaCrSb_3$ was observed to have a non-collinear magnetic configuration at low temperature [13]. There are a high moment FM coupling along the lattice vector **b** and a small moment antiferromagnetic (AFM) coupling along the lattice vector **c**. The magnetic moment of the FM sublattice is 1.65 μ_B/f.u. and that of the AFM sublattice is 0.49 μ_B/f.u. [13]. There have been several theoretical works

*mcnguyen@ameslab.gov

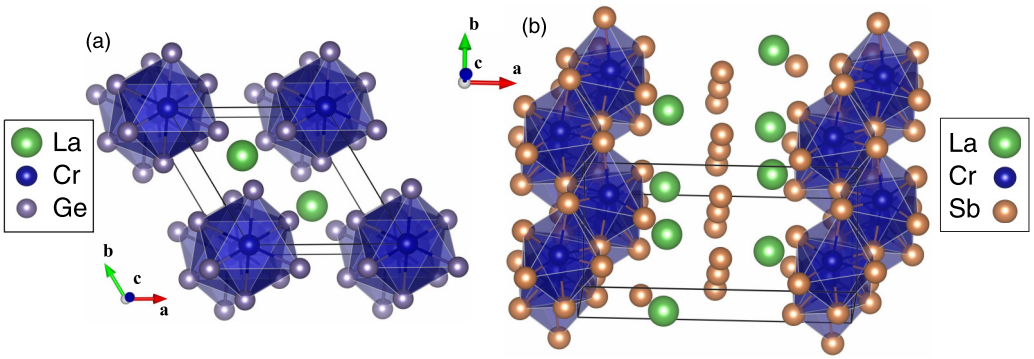

FIG. 1. Atomic structure of (a) $LaCrGe_3$ and (b) $LaCrSb_3$. Some atoms in both structures and unit cells of $LaCrSb_3$ are repeated to show the one- and two-dimensional features of Cr in $LaCrGe_3$ and $LaCrSb_3$, respectively.

on $LaCrGe_3$ and $LaCrSb_3$ based on density functional theory [14–18], where all of them focused on electronic and magnetic properties of materials at ambient pressure.

Our first-principles calculations show that at ambient pressure $LaCrGe_3$ is a simple FM and $LaCrSb_3$ exhibits a noncollinear magnetic configuration, consistent with the experimental reports. Both systems are mechanically stable and quite compressible (especially $LaCrSb_3$) in comparison with typical metals. In the pressure dependence investigation, we first take only FM and nonmagnetic (NM) phases into consideration identifying the magnetism in $LaCrGe_3$ as fragile in comparison with that of $LaCrSb_3$. The key controlling parameter to the magnetic properties of $LaCrGe_3$ under pressure is the distance between Cr atoms so the effects of hydrostatic and uniaxial pressures on magnetic moment are very similar.

II. COMPUTATIONAL AND EXPERIMENTAL METHODS

The first-principles spin-polarized density functional theory (DFT) [19] calculations are performed using the plane-wave basis Vienna Ab Initio Simulation Package (VASP) [20] with the projector-augmented wave pseudopotential method [21,22] within the local density approximation parameter by Perdew and Zunger [23,24]. The energy cutoff is 450 eV and the Monkhorst-Pack scheme [25] is used for Brillouin-zone sampling. A dense k-point grid of $2\pi \times 0.025\,\text{Å}^{-1}$ is used in all calculations, except for density of states (DOS) calculations where a 1.5 times denser k-point mesh is used for accurate DOS. All structures are fully relaxed until the forces acting on each atom are smaller than $0.01\,\text{eV/Å}$ and pressures are smaller than 0.1 GPa. The energy convergence criterion is 10^{-5} eV. The total enthalpy is calculated as $H = E + PV$, where E is the total energy, P is the external pressure, and V is the system volume. The noncollinear spin-polarization and spin-orbit coupling (SOC) interaction [26] are included in some calculations for $LaCrSb_3$ at ambient pressure where noted. All other calculations are collinear spin-polarized without spin-orbit coupling except where it is clearly indicated. In our experiment, single crystals of $LaCrGe_3$ and $LaCrSb_3$ were grown from solutions as reported in Refs. [2,3,5,27]. The magnetization measurements under pressure were performed using a moissanite anvil cell [28]. Daphne 7474 was used as a pressure medium [29], and the pressure was determined at 77 K by the ruby fluorescence technique [30].

III. RESULTS AND DISCUSSION

A. Physical properties of $LaCrGe_3$ and $LaCrSb_3$ at ambient condition

We first discuss the structural and magnetic properties of $LaCrGe_3$ and $LaCrSb_3$ at ambient conditions. In our calculations, FM, NM, and different AFM structures are studied in order to verify the experimentally observed ground structures. Specifically, for $LaCrGe_3$, we consider AFM structure along the c axis. For $LaCrSb_3$ both AFM along the b axis (b-AFM) and c axis (c-AFM) structures are considered. We list the lattice parameters of $LaCrGe_3$ and $LaCrSb_3$ in all magnetic structures as well as from experiment and previous calculations in Table I. Our calculations confirm that the FM structure is the most stable one for both $LaCrGe_3$ and $LaCrSb_3$. In the $LaCrGe_3$ system, the FM structure is $-34.9\,\text{meV/f.u.}$ lower in energy than the NM structure, which is consistent with previous calculation [18]. The AFM structure cannot be stabilized and it converged to a NM structure in our calculation. For $LaCrSb_3$ within collinear magnetism without SOC interaction, the FM structure is -48.3, -46.4 and $-101.2\,\text{meV/f.u.}$ lower in energy than the b-AFM, c-AFM, and NM structures, respectively, consistent with experiment and previous calculation [14]. We note that a previous calculation by Choi *et al.* [15] predicted that the FM phase is a metastable structure. Their calculations showed that c-AFM is more stable than both b-AFM and FM structures.

As one can see from Table I, the local-density approximation (LDA) calculated lattice parameters of FM $LaCrGe_3$ are slightly smaller than those from experiment at 1.7 K [31],

TABLE I. Lattice parameters from experiment and calculations ($T = 0\,\text{K}$) for different magnetic configurations of $LaCrGe_3$ and $LaCrSb_3$.

	$LaCrGe_3$ ($Z = 2$)		$LaCrSb_3$ ($Z = 4$)		
	a (Å)	c (Å)	a (Å)	b (Å)	c (Å)
Expt.	6.165	5.748	13.264	6.182	6.094
	at $T = 1.7\,\text{K}$		at $T = 5.0\,\text{K}$		
FM	6.078	5.587	13.043	6.115	5.958
b-AFM	N/A		13.003	6.109	5.948
c-AFM			13.003	6.119	5.955

TABLE II. Magnetic moment of Cr atom (μ_B) and total magnetic moment of $LaCrGe_3$ (μ_B/f.u.) and $LaCrSb_3$ from current (within LDA, LDA with experimental lattice constant, and LDA + SOC) and previous calculations. The methods used in previous calculations are also shown.

		$LaCrGe_3$		$LaCrSb_3$	
		M_{Cr}	M_{tot}	M_{Cr}	M_{tot}
Expt.			1.22 ∼ 1.25		1.61 ∼ 1.72
This work	LDA	1.17	1.09	1.65	1.55
	LDA expt. latt.	1.28	1.16	1.91	1.80
	LDA + SOC	1.20	1.12	1.70	1.55
Previous works			1.30 (TB–LMTO)[a]	2.81[b,c] (LMTO)	2.39[c] (LMTO) 2.10[d] (FPLO)

[a]Reference [18].
[b]Reference [14].
[c]Reference [15].
[d]Reference [16].

1.4% and 2.8% smaller for a and c parameters, respectively. The results are similar for $LaCrSb_3$ where LDA slightly underestimates the FM lattice parameters, within 2.2% difference from experiment at 5 K [32]. We note that DFT calculations are at 0 K but the thermal expansion effect on the lattice parameter comparison should be negligible as experimental data are collected at very low temperature as mentioned above. All previous theoretical work on $LaCrSb_3$ used experimental lattice parameters [15–17] so there are no other DFT relaxed lattice parameters to compare with our results. $LaCrGe_3$ has been synthesized in experiment recently so, apart from our work [5], there is only one theoretical work on $LaCrGe_3$ [18], which also used experimental lattice parameters.

Table II shows the magnetic moment of Cr atom in $LaCrGe_3$ and $LaCrSb_3$ from experiment [2,3,13,31,33], our calculations, and previously available calculations. Previous calculations were performed by linear muffin-tin orbital (LMTO) band method [15], tight-binding LMTO [18], or full-potential local-orbital (FPLO) method [16]. In our calculations, the magnetic moment of Cr atom is 1.17 μ_B in $LaCrGe_3$ and 1.65 μ_B in $LaCrSb_3$. The magnetic moments of La and Ge/Sb are AFM coupled with those of Cr, so the total magnetic moment is slightly smaller than the magnetic moment of the Cr atom. From Table II we can see that magnetic moments are reproduced well in our LDA calculations for both $LaCrGe_3$ and $LaCrSb_3$. The total magnetic moments of $LaCrGe_3$ and $LaCrSb_3$ are slightly underestimated in comparison with experiment. Note that all previous calculations substantially overestimated the magnetic moment of $LaCrSb_3$, especially for LMTO calculation. The large overestimation of Cr moment in $LaCrSb_3$ in LMTO calculations might be due to the choice of basis set and muffin-tin radii, as it is shown that different LMTO calculation settings [14,15] can give different relative stability between magnetic phases. For a better and direct comparison with previous studies, we also perform calculations with experimental lattice parameters. In this case the magnetic moment appears to be slightly larger in comparison with those of relaxed structures by LDA but still agrees well with the experiment. This enlargement of magnetic moment is directly related to the underestimation of lattice parameter of LDA. The difference between our calculations and previous ones, especially for $LaCrSb_3$, could be due to implementations of LDA as mentioned above.

Figures 2 and 3 show band structures for majority and minority spin and projected density of states (PDOS) on Cr d orbitals of FM $LaCrGe_3$ and FM $LaCrSb_3$, respectively. The positive and negative DOS values are corresponding majority- and minority-spin PDOS. We find that the main contributions to the DOS near Fermi level are from Cr d orbital in both systems. There are very strong Cr d orbitals PDOS peaks just below the Fermi level in the majority-spin channel of $LaCrGe_3$. The flat bands running through the Γ-M-K-Γ segment of majority-spin band structure are responsible for this strong peak. As will be seen later, the first occupied peak, count from Fermi level, of

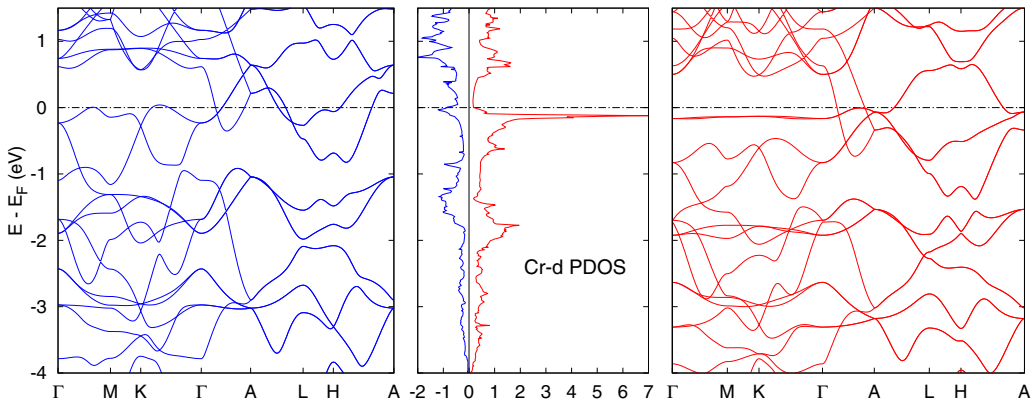

FIG. 2. Band structures of (left) minority- and (right) majority spin and (middle) DOS of Cr d orbitals of $LaCrGe_3$.

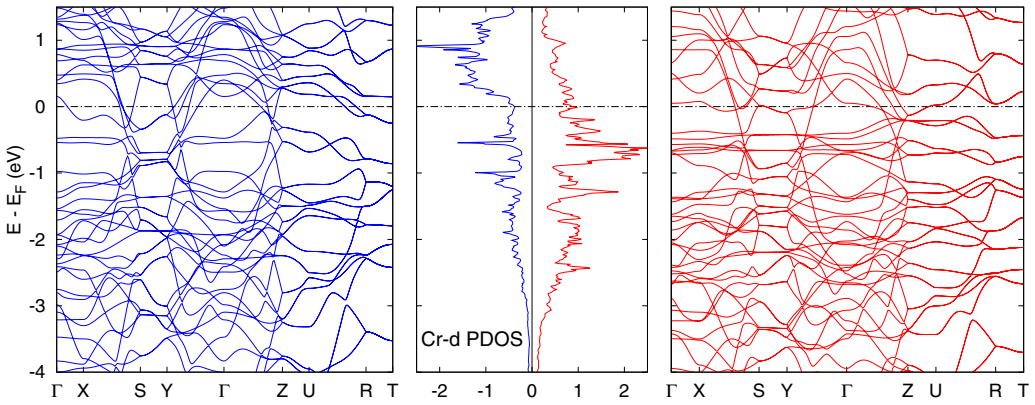

FIG. 3. Band structures of (left) minority- and (right) majority spin and (middle) DOS of Cr d orbitals of $LaCrSb_3$.

$LaCrGe_3$, is much closer to Fermi level than that of $LaCrSb_3$, and its proximity to the Fermi level is responsible for the magnetic fragility of $LaCrGe_3$. The unoccupied minority spin bands at ∼0.8 eV are also quite flat and they correspond to a PDOS peak in minority spin channel at ∼0.8 eV above Fermi level. There is also a small DOS peak of Cr d orbitals in minority spin channel very close to Fermi level.

For $LaCrSb_3$, the contribution from Cr d orbitals is dominating for the first main peak from −0.4 to −0.8 eV of majority-spin DOS. There are very flat bands running through the Γ-X-S-Y-Γ-Z segment of majority-spin band structure. These bands induce the peaks in majority-spin DOS around −0.4 and −0.6 eV. There are also quite flat band going through the Γ-X-S and Γ-Z segments of majority-spin band structure and they are responsible for peaks near −0.8 eV. The unoccupied minority-spin bands of these orbitals at ∼0.9, ∼0.6, and ∼0.3 eV are also quite flat and pure as well and they are corresponding to DOS peaks in minority spin at ∼0.9, ∼0.6 and ∼0.3 eV above Fermi level.

As mentioned above, the neutron scattering experiment observed a noncollinear magnetic structure for $LaCrSb_3$ [13]. To investigate the effects of noncollinearity, we perform self-consistent noncollinear magnetic calculations in LDA, i.e., allowing the magnitude of magnetic moment in all directions (i.e., x, y, and z) to change freely, for $LaCrSb_3$ with the above relaxed lattice parameters. Several calculations are performed independently with different initial magnetic moments to make sure we obtained the global stable state but not a local minimum. All symmetries are turned off for these calculations. Since La is a relatively heavy element, the SOC interaction is included in the noncollinear calculation. The obtained magnetic configuration for $LaCrSb_3$ consists of a FM sublattice along the b axis and an AFM sublattice along the c axis with a magnitude of Cr magnetic moment of 1.66 and 0.38 μ_B/Cr for each sublattice, respectively, which is in very good agreement with experiment. Our analysis revealed that such a magnetic configuration is formed by the interplay between nearest- and next-nearest-neighbor Cr-Cr exchange interactions: a positive (FM) next-nearest-neighbor interaction in the (a, b) plane and a negative (AFM) nearest-neighbor interaction along the c axis. This is somewhat similar to the spin reorientational transition mechanism in Invar systems proposed by Antropov *et al.* [34]. Thus, this frustration is a leading mechanism of magnetic structure formation in this system. These results again show that LDA as implemented in VASP can describe the $LaCrSb_3$ system reasonably well. We also perform the noncollinear including SOC interaction calculation for $LaCrGe_3$ to investigate the effect of SOC interaction on the magnetic moment of Cr. We find that magnetic moments of Cr are collinear and slightly enhanced from their value of 1.17 μ_B in calculation without SOC interaction to 1.20 μ_B. The obtained orbital moments of all atoms in $LaCrGe_3$ and $LaCrSb_3$ are practically zero.

There have been no investigations on elastic and mechanical properties of $LaCrGe_3$ and $LaCrSb_3$. All previous work are on electronic and magnetic properties [14–18]. In this work, we also investigate elastic and mechanical properties of $LaCrGe_3$ and $LaCrSb_3$ in the thermodynamic ground states of FM. The elastic constants are calculated based on the stress-strain relationship approach [35]. The Voigt (subscript V) and Reuss (subscript R) bounds of bulk (B) and shear (G) moduli are calculated by the following formulas [36]:

$$B_V = (1/9)[2(C_{11} + C_{12}) + 4C_{13} + C_{33}],$$
$$G_V = (1/30)(M + 12C_{44} + 12C_{66}),$$
$$B_R = C^2/M,$$
$$G_R = (5/2)(C^2 C_{44} C_{66})/[3B_v C_{44} C_{66} + C^2(C_{44} + C_{66})],$$

where $M = C_{11} + C_{12} + 2C_{33} - 4C_{13}$ and $C^2 = [(C_{11} + C_{12})C_{33} - 2C_{13}^2]$ for hexagonal $LaCrGe_3$.

$$B_V = (1/9)[C_{11} + C_{22} + C_{33} + 2(C_{12} + C_{13} + C_{23})],$$
$$G_V = (1/15)[C_{11} + C_{22} + C_{33} + 3(C_{44} + C_{55} + C_{66}) - (C_{12} + C_{13} + C_{23})],$$
$$B_R = \Delta/[C_{11}(C_{22} + C_{33} - 2C_{23}) + C_{22}(C_{33} - 2C_{13}) - 2C_{33}C_{12} + C_{12}(2C_{23} - C_{12}) + C_{13}(2C_{12} - C_{13}) + C_{23}(2C_{13} - C_{23})],$$
$$G_R = 15/\{4[C_{11}(C_{22} + C_{33} + C_{23}) + C_{22}(C_{33} + C_{13}) + C_{33}C_{12} - C_{12}(C_{23} + C_{12}) - C_{13}(C_{12} + C_{13}) - C_{23}(C_{13} + C_{23})]/\Delta + 3[(1/C_{44} + 1/C_{55} + 1/C_{66})]\},$$

where $\Delta = C_{13}(C_{12}C_{23} - C_{13}C_{22}) + C_{23}(C_{12}C_{13} - C_{23}C_{11}) + C_{33}(C_{11}C_{22} - C_{12}^2)$ for orthorhombic $LaCrSb_3$.

The arithmetic averaged values of bulk or shear moduli from Voigt and Reuss bounds are the corresponding Voigt-Reuss-Hill approximation of bulk or shear moduli, respectively.

TABLE III. Elastic constants of $LaCrGe_3$ and $LaCrSb_3$.

	$LaCrGe_3$ (GPa)	$LaCrSb_3$ (GPa)
C_{11}	243.8	133.6
C_{12}	64.9	41.5
C_{13}	58.7	41.7
C_{22}	243.8	163.9
C_{23}	58.7	34.6
C_{33}	204.9	170.0
C_{44}	80.3	56.0
C_{55}	80.3	55.6
C_{66}	89.5	47.6
B_V/B_R	117.5/116.5	78.1/77.6
G_V/G_R	84.0/83.7	55.2/54.4
E_H	203.1	113.1

Within Voigt-Reuss-Hill approximation, Young's modulus (E) is calculated as

$$E_H = 9B_H G_H/(3B_H + G_H).$$

The results from our calculations for elastic constants and moduli of $LaCrGe_3$ and $LaCrSb_3$ are shown in Table III. All moduli of $LaCrSb_3$ are quite smaller than those of $LaCrGe_3$. Comparing with other typical metals, moduli of $LaCrSb_3$ are comparable to those of Zn. The shear and Young's moduli of $LaCrGe_3$ are comparable to those of Co and Ni but its bulk modulus is only about two-thirds of those of Co and Ni. From elastic constants in Table III we can verify easily that both $LaCrGr_3$ and $LaCrSb_3$ are mechanically stables as their elastic constants obey the corresponding Born mechanical stability criteria [36,37]:

$C_{44} > 0$, $C_{11} > |C_{12}|$, and $(C_{11} + 2C_{12})C_{33} > 2C_{13}^2$ for hexagonal $LaCrGe_3$ or

$C_{ii} > 0 (i = 1,6)$, $[C_{11} + C_{22} + C_{33} + 2(C_{12}+C_{13}+C_{23})] > 0$, $(C_{11} + C_{22} - 2C_{12}) > 0$, $(C_{11} + C_{32} - 2C_{13}) > 0$ and $(C_{22} + C_{33} - 2C_{23}) > 0$ for orthorhombic $LaCrSb_3$.

B. Pressure dependence of magnetic moments of $LaCrGe_3$ and $LaCrSb_3$

We have also performed calculations to investigate the stability of FM phases of $LaCrGe_3$ and $LaCrSb_3$ under external pressure. The formation enthalpy differences between FM and NM phases of $LaCrGe_3$ and $LaCrSb_3$ are shown as functions of external pressure in Fig. 4. We also show in this figure the pressure dependence of magnetic moments of Cr atom in $LaCrGe_3$ and $LaCrSb_3$. The FM phases of $LaCrGe_3$ and $LaCrSb_3$ are seen to be fully suppressed by pressures of about 7 and 30 GPa, respectively. The magnetic moment of Cr in $LaCrGe_3$ is decreasing slightly with external pressure, within 10% from 1.17 μ_B at ambient condition to 1.08 μ_B at 6 GPa, before the NM phase becoming stable at 7 GPa. For $LaCrSb_3$, when the external pressure is increasing, the magnetic moment of Cr is decreasing more rapidly, but the FM phase will transform to another lower-moment FM phase

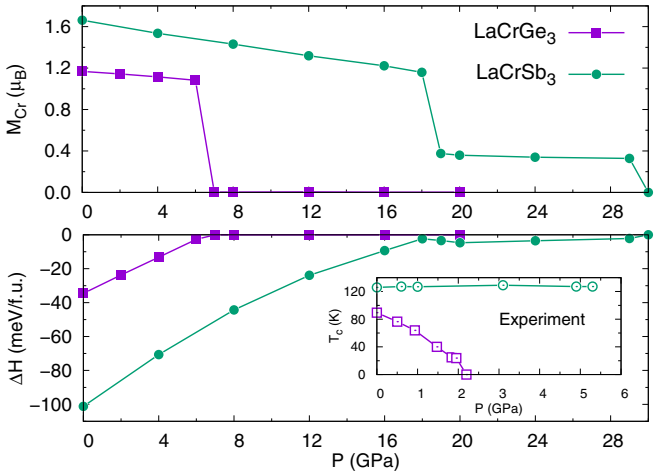

FIG. 4. Formation enthalpy differences between FM and NM phases and magnetic moment of Cr atom as functions of pressure for $LaCrGe_3$ and $LaCrSb_3$. The inset shows the experimental results for the dependence of $LaCrGe_3$ and $LaCrSb_3$ T_c on pressure [3,5].

before finally transforming to NM phase. The first transition pressure, from high- to low-moment FM, is 18 GPa and the second transition pressure, from low-moment FM to NM, is 30 GPa. The magnetic moment of the Cr atom in high-moment FM phase is decreasing with pressure and it is decreasing almost linearly. For low-moment FM phase of $LaCrSb_3$, there is a very small bump in the formation enthalpy difference. It increases slightly first, then decreases with pressure. The formation enthalpy difference of $LaCrSb_3$ at 19 GPa is -2 meV/f.u. and it has a dip of -4 meV/f.u. at 20 GPa (Fig. 4). It should be noted that these small enthalpy differences are within the accuracy of DFT calculations. The magnetic moment of Cr atom in $LaCrSb_3$ low-moment FM phase decreases slightly with external pressure between 19 and 29 GPa.

In the inset of Fig. 4 we also show the experiment results for the dependence of Curie temperature (T_c) of $LaCrGe_3$ and $LaCrSb_3$ on external pressure up to 6 GPa [3,5]. The experimental results show that the FM phase of $LaCrGe_3$ becomes unstable at 2.2 GPa and there is no sign of magnetic transition in $LaCrSb_3$ up to 6.0 GPa, the high-pressure limit in our experiment. Our present theoretical calculation results are consistent with experiment that $LaCrGe_3$ is a fragile magnet where its ferromagnetism can be suppressed with small external pressure, whereas $LaCrSb_3$ is not fragile magnetically and requires a very high pressure to suppress its ferromagnetism. These results indicate that first-principles DFT calculation is able to predict the magnetic fragility of FM materials and it can be used to screen potential fragile FM compounds under external pressure to guide experiment explorations. However, we can see clearly an overestimation of the transition pressure from our calculation for $LaCrGe_3$. We would like to note that phase-transition pressure from DFT calculation sometimes can be systematically off from the experimental value, but the trend of pressure-dependent phase transition usually can be well described. For example, the predicted structural transition pressure of Si from carbon diamond (Si-I) to β-Sn (Si-II) phase is several GPa different from the experimental value, depending on the exchange-correlation functional used [38,39]. But

the sequence of phase transitions, i.e., Si-I to Si-II to Si-V to Si-VI to Si-VII, from DFT calculations is consistent with experiment [38]. The DFT calculation, therefore, is expected to be able to predict well the magnetic phase transition sequence. The second possible source of the overestimation of transition pressure from our calculations is the appearance of various AFM phases, so the magnetic phase transition could be from FM phase to AFM [5] or even some noncollinear phase [34] instead of NM phase. This is due to possible importance of metallic spin fluctuations in such metals [40] especially near magnetic phase transition. However, in the current section, only FM and NM phases are taken into account. While the analysis of the DOS can be profitable for the discussion of FM-state stability, the possible presence of other magnetic states requires the knowledge of magnetic susceptibility at all wave vectors. In general, such analysis of magnetic susceptibility and the account of spin fluctuations can be important but it goes beyond the DFT treatment we employed in this paper. We plan to address this issue in our future publications. We also show later that for $LaCrGe_3$, the appearance of AFM phases can lower the transition pressure. From Fig. 4 we also observe that for $LaCrGe_3$ there is a correlation between magnetic moment and T_c as both are decreasing with pressure. However, there seems to be no clear correlation between the magnetic moment and T_c of $LaCrSb_3$ under pressure. The T_c of $LaCrSb_3$ is almost constant with pressure up to 6 GPa in experiment.

The Cr in $LaCrGe_3$ forms a pseudo-1D structure along the c axis since the distance between Cr atoms along the c axis is 2.79 Å, which is much smaller than the distance between Cr atoms in the basal plane (6.078 Å). This implies that the magnetic interaction between Cr atoms is mainly between Cr atoms along the c axis, meaning that the magnetic properties of the $LaCrGe_3$ under hydrostatic pressure and that of hypothetically uniaxially strained $LaCrGe_3$ should be very similar as long as they have the same Cr-Cr distance along the c axis. In other words, we would see very similar ordered Cr magnetic moments for these two systems. In order to verify this, we change the length of lattice vector **c** manually and fully relax the lattice vectors **a** and **b** and internal atomic coordinates of $LaCrGe_3$ to calculate the magnetic moment of Cr. This simulation is equivalent to directional compression or uniaxial pressure experiment where the $LaCrGe_3$ system is compressed along the c axis. Thus, an experiment can be performed to verify our calculation prediction. The results of Cr magnetic moment of uniaxial pressure-compressed $LaCrGe_3$ together with the results for $LaCrGe_3$ under hydrostatic pressure from the above calculations as functions of the distance between Cr atoms along the c axis are shown in Fig. 5. In this figure, we also show the magnetic moment of Cr in $LaCrGe_3$ under negative pressure to compare with that of Cr in $LaCrGe_3$ under directional elongation. It is interesting that the magnetic moments of Cr in $LaCrGe_3$ under hydrostatic pressure fall almost perfectly on the magnetic moments curve of Cr in $LaCrGe_3$ under directional compression/elongation, reconfirming that Cr in $LaCrGe_3$ is indeed essentially one dimensional in terms of the magnetic interaction.

These results show that for systems with one-dimensional magnetic moment bearing atoms the effects of hydrostatic and uniaxial pressures on magnetic properties could be very close.

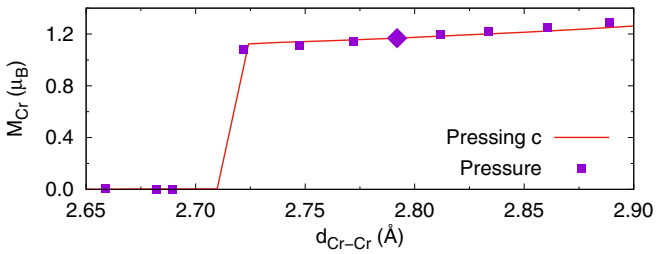

FIG. 5. Magnetic moment of Cr as function of distance between Cr atom along the c axis of $LaCrGe_3$ under hydrostatic pressure and pressing along the c axis. Diamond-marked point is for systems at ambient condition.

Therefore, uniaxial pressure can be used as another method to suppress magnetism in the systems with magnetic atoms arranged in one-dimensional fashion, although experimentally the range of accessible uniaxial pressures is significantly smaller than that of hydrostatic or quasihydrostatic pressures. The different exotic phenomena could be emerging from magnetic materials with one-dimensional magnetic atoms when hydrostatic pressure or uniaxial pressure is applied.

In order to understand more physics of the transition from FM to NM phase of $LaCrGe_3$ under pressure, PDOS of Cr in $LaCrGe_3$ under different hydrostatic and uniaxial pressures are calculated. Figure 6 shows the Cr PDOS at ambient condition and under hydrostatic pressure of 6 and 7 GPa. The figure's inset shows the Cr PDOS of $LaCrGe_3$ under uniaxial pressure along lattice vector **c**. The Cr-Cr distances in $LaCrGe_3$ structure with $c/c_0 = 0.98$ and 0.97 are very close to that of $LaCrGe_3$ under hydrostatic pressure of 6 and 7 GPa, respectively, where c_0 and c are the lengths of lattice vector **c** at ambient condition and under uniaxial pressure. We can see clearly from Fig. 6 that when $LaCrGr_3$ is more and more compressed under either hydrostatic or uniaxial pressure, the very high Cr PDOS peak, which is just below (about -0.15 eV) the Fermi level at ambient condition, is pushed closer and closer to the Fermi level. When this peak crosses the Fermi level, somewhere between 6 and 7 GPa or between $c/c_0 = 0.98$ and 0.97, it introduces a peculiar instability to the FM phase due to very high DOS of one spin channel at Fermi level. This instability

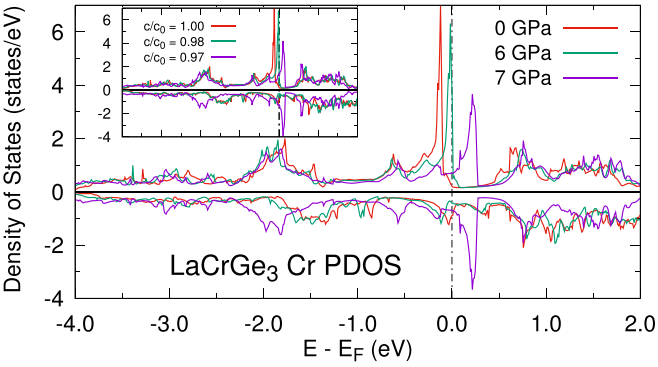

FIG. 6. PDOS of Cr in $LaCrGe_3$ under hydrostatic pressure and (in the inset) uniaxial pressure. PDOS of NM $LaCrGe_3$ at 7 GPa and $c/c_0 = 0.97$ are plotted as half positive and half negative for better comparison.

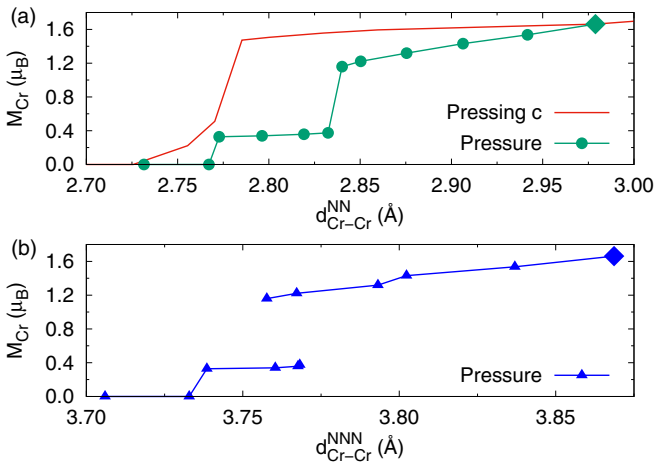

FIG. 7. Magnetic moment of Cr as functions (a) NN and (b) NNN distance of Cr-Cr NN in $LaCrSb_3$ under hydrostatic pressure and pressing along the c axis. Diamond-marked points are for system at ambient condition.

will induce a magnetic or structural transition. We do not observe any structural transition as the symmetries are the same at 6 and 7 GPa and at $c/c_0 = 0.98$ and 0.97. The magnetic phase transition could be from FM phase to a noncollinear magnetic, an AFM, or a NM phase. Since we do not consider noncollinear and AFM phases in this work, what kind of magnetic phase transition cannot be resolved precisely. However, the important observation here is that the FM phase is destabilized by the high Cr PDOS peak at Fermi level. Comparing Cr PDOS of $LaCrGe_3$ at 6 and 7 GPa or between $c/c_0 = 0.98$ and 0.97 in Fig. 6, we can see a splitting of the strong Cr majority-spin PDOS peak into an unoccupied peak at about 0.20 eV and other two occupied peaks at about −0.50 and around −1.90 eV. We obtain a similar FM to NM transition picture in $LaCrSb_3$ for the first majority-spin PDOS center at ∼−0.75 eV. Thus, the proximity of a strong DOS peak to Fermi level in $LaCrGe_3$ makes the FM phase fragile and it may be used as an indicator for screening of ferromagnetic fragile materials.

At this point, one may ask whether $LaCrSb_3$ shows the same magnetic behavior under uniaxial and hydrostatic pressure as we observed in the $LaCrGe_3$ system above. As can be seen from Fig. 7(a), the magnetic moment of Cr in $LaCrSb_3$ under hydrostatic pressure and that of $LaCrSb_3$ under uniaxial pressure are resolvedly different in terms of dependence on Cr-Cr distance along the c axis. This result is expected as we mentioned above that Cr in $LaCrSb_3$ forms a pseudo-2D structure instead of 1D as that in $LaCrGe_3$. For $LaCrSb_3$ at ambient condition, the distance between Cr atoms along the c axis [which is the Cr-Cr nearest neighbor (NN)] is 2.98 Å, while the nearest distance between Cr atoms in the (a, b) plane [which is the Cr-Cr next-NN (NNN)] is 3.93 Å, which is not much larger than the NN distance. Therefore, there is interplay between the NN and NNN Cr-Cr interactions. Under the hydrostatic pressure, both the Cr-Cr NN and NNN distances of FM $LaCrSb_3$ would decrease with pressure, whereas the latter one is increasing as we apply uniaxial pressure along the c axis on FM $LaCrSb_3$ in order to release stresses induced by compression of the c axis. These differences in the Cr-Cr NNN distances induce different behavior of the NNN Cr-Cr interactions and thus the magnetic moment of Cr. As can be seen in Fig. 7(a), the magnetic moments of Cr atom in hydrostatic and uniaxial pressure cases diverge from the starting point of ambient condition. A closer look at the change of Cr-Cr NN and NNN distances of $LaCrSb_3$ under hydrostatic pressure, shows there is an abrupt bump of the NNN distance at the transition from high-spin to low-spin state [Fig. 7(b)], while the NN distance is decreasing monotonically with pressure. We do not observe any sudden opposite direction change of the Cr-Cr NNN distance in the uniaxial pressure case. These results imply that the bump of the Cr-Cr NNN distance could be responsible for stabilizing the low-spin state and a steplike behavior of magnetic moment of $LaCrSb_3$ under hydrostatic pressure. Figure 7(b) also shows the coexistence of low ($0.4\,\mu_B$) and high ($1.2\,\mu_B$) spin ferromagnetic configurations near NNN distance ∼3.77 Å and hysteretic type of behavior for magnetization. In this area more complex magnetic states may exist. A comparison of DOS of $LaCrSb_3$ at 20 GPa to that at 18 GPa shows that, apart from some minor differences in DOS profiles, the up- (down-) spin DOS is shifted to the right (left) of Fermi level, changing the occupation of each spin channel. This explains the calculated magnetic moment is lower in the higher-pressure FM phase.

Recently, further detailed investigations of resistivity and muons spin spectroscopy [5] on the pressure-phase diagram of $LaCrGe_3$ found evidence for the appearance of modulated AFM phases. The appearance of the modulated AFM phases would lower the pressure with the FM phase being depressed since AFM phases could become more stable than the FM phase at lower pressure before the NM phase becomes stable. Indeed, as was shown in Ref. [5], AFM orders with small q vectors can become more stable than the FM phase and hence reduce the pressure at which the FM disappears. This demonstrates the possibility of an ideal integration between first-principles calculations and experiments: the calculations can identify which material is likely to show fragile magnetism; the experiments can discover unexpected phases which can then be considered in the calculations.

IV. CONCLUSIONS

In summary, we have investigated elastic, mechanic, electronic, and magnetic properties of $LaCrGe_3$ and $LaCrSb_3$ by first-principles density functional theory calculations. Overall the DFT results are consistent with experiments. $LaCrGe_3$ has a ferromagnetic ground state, while the $LaCrSb_3$ ground state consists of a ferromagnetic sublattice with moment parallel to lattice vector **b** and an antiferromagnetic sublattice with a quite smaller moment parallel to lattice vector **c**. First-principles calculations can be used for screening for fragile FM phases by considering FM and NM phases. When various AFM phases are considered, first principles can predict accurately the transition pressure of the FM phase of $LaCrGe_3$ at ∼2 GPa [5]. The key parameter for a magnetic system with one-dimensional magnetic atoms is the distance between them, so the effects of hydrostatic and uniaxial pressures on magnetic moment are very similar. The proximity of

the $LaCrGe_3$ high DOS peak to Fermi level makes the FM phase fragile.

ACKNOWLEDGMENTS

This work was supported by the U.S. Department of Energy (DOE), Office of Science, Basic Energy Sciences, Materials Science and Engineering Division, including computing time at the National Energy Research Scientific Computing Center (NERSC). The research was performed at the Ames Laboratory, which is operated for the U.S. DOE by Iowa State University under Contract No. DE-AC02-07CH11358. Magnetization measurements under pressure (V.T.) were supported by Ames Laboratory's laboratory-directed research and development funding.

[1] V. Taufour, D. Aoki, G. Knebel, and J. Flouquet, Phys. Rev. Lett. **105**, 217201 (2010).
[2] X. Lin, V. Taufour, S. L. Bud'ko, and P. C. Canfield, Phys. Rev. B **88**, 094405 (2013).
[3] X. Lin, V. Taufour, S. L. Bud'ko, and P. C. Canfield, Philos. Mag. **94**, 1277 (2014).
[4] P. C. Canfield and S. L. Bud'ko, Rep. Prog. Phys. **79**, 084506 (2016).
[5] V. Taufour, U. S. Kaluarachchi, R. Khasanov, M. C. Nguyen, Z. Guguchia, P. K. Biswas, P. Bonfà, R. De Renzi, X. Lin, S. K. Kim, E. D. Mun, H. Kim, Y. Furukawa, C.-Z. Wang, K.-M. Ho, S. L. Bud'ko, and P. C. Canfield, Phys. Rev. Lett. **117**, 037207 (2016).
[6] G. G. Lonzarich, S. S. Saxena, P. Agarwal, K. Ahilan, F. M. Grosche, R. K. W. Haselwimmer, M. J. Steiner, E. Pugh, I. R. Walker, S. R. Julian, P. Monthoux, A. Huxley, I. Sheikin, D. Braithwaite, and J. Flouquet, Nature (London) **406**, 587 (2000).
[7] H. v. Löhneysen, A. Rosch, M. Vojta, and P. Wölfle, Rev. Mod. Phys. **79**, 1015 (2007).
[8] E. Colombier, S. L. Bud'ko, N. Ni, and P. C. Canfield, Phys. Rev. B **79**, 224518 (2009).
[9] S. K. Kim, M. S. Torikachvili, E. Colombier, A. Thaler, S. L. Bud'ko, and P. C. Canfield, Phys. Rev. B **84**, 134525 (2011).
[10] J. J. Wu, J.-F. Lin, X. C. Wang, Q. Q. Liu, J. L. Zhu, Y. M. Xiao, P. Chow, and C. Jin, Proc. Natl. Acad. Sci. U.S.A. **110**, 17263 (2013).
[11] U. S. Kaluarachchi, V. Taufour, A. Sapkota, V. Borisov, T. Kong, W. R. Meier, K. Kothapalli, B. G. Ueland, A. Kreyssig, R. Valentí, R. J. McQueeney, A. I. Goldman, S. L. Bud'ko, and P. C. Canfield, Phys. Rev. B **96**, 140501 (2017).
[12] J. Paglione and R. L. Greene, Nat. Phys. **6**, 645 (2010).
[13] E. Granado, H. Martinho, M. S. Sercheli, P. G. Pagliuso, D. D. Jackson, M. Torelli, J. W. Lynn, C. Rettori, Z. Fisk, and S. B. Oseroff, Phys. Rev. Lett. **89**, 107204 (2002).
[14] J. H. Shim and B. I. Min, J. Magn. Magn. Mater. **272-276**, E241 (2004).
[15] H. C. Choi, J. H. Shim, S. K. Kwon, and B. I. Min, J. Appl. Phys. **101**, 09G513 (2007).
[16] M. Richter, J. Rusz, H. Rosner, K. Koepernik, I. Opahle, U. Nitzsche, and H. Eschrig, J. Magn. Magn. Mater. **272-276**, E251 (2004).
[17] M. P. Ghimire, Sandeep, T. P. Sinha, and R. K. Thapa, Solid State Commun. **151**, 1224 (2011).
[18] H. Bie, O. Y. Zelinska, A. V. Tkachuk, and A. Mar, Chem. Mater. **19**, 4613 (2007).
[19] W. Kohn and L. J. Sham, Phys. Rev. **140**, A1133 (1965).
[20] G. Kresse and J. Furthmüller, Phys. Rev. B **54**, 11169 (1996).
[21] P. E. Blöchl, Phys. Rev. B **50**, 17953 (1994).
[22] G. Kresse and D. Joubert, Phys. Rev. B **59**, 1758 (1999).
[23] J. P. Perdew and A. Zunger, Phys. Rev. B **23**, 5048 (1981).
[24] D. M. Ceperley and B. J. Alder, Phys. Rev. Lett. **45**, 566 (1980).
[25] H. J. Monkhorst and J. D. Pack, Phys. Rev. B **13**, 5188 (1976).
[26] S. Steiner, S. Khmelevskyi, M. Marsmann, and G. Kresse, Phys. Rev. B **93**, 224425 (2016).
[27] U. S. Kaluarachchi, S. L. Bud'ko, P. C. Canfield, and V. Taufour, Nat. Commun. **8**, 546 (2017).
[28] P. Lebre Alireza, S. Barakat, A.-M. Cumberlidge, G. Lonzarich, F. Nakamura, and Y. Maeno, J. Phys. Soc. Jpn. **76**, 216 (2007).
[29] K. Murata, K. Yokogawa, H. Yoshino, S. Klotz, P. Munsch, A. Irizawa, M. Nishiyama, K. Iizuka, T. Nanba, T. Okada, Y. Shiraga, and S. Aoyama, Rev. Sci. Instrum. **79**, 085101 (2008).
[30] G. J. Piermarini, S. Block, J. D. Barnett, and R. A. Forman, J. Appl. Phys. **46**, 2774 (1975).
[31] J. M. Cadogan, P. Lemoine, B. R. Slater, A. Mar, and M. Avdeev, Solid State Phenom. **194**, 71 (2013).
[32] N. P. Raju, J. E. Greedan, M. J. Ferguson, and A. Mar, Chem. Mater. **10**, 3630 (1998).
[33] D. D. Jackson, M. Torelli, and Z. Fisk, Phys. Rev. B **65**, 014421 (2001).
[34] V. P. Antropov, M. I. Katsnelson, B. N. Harmon, M. van Schilfgaarde, and D. Kusnezov, Phys. Rev. B **54**, 1019 (1996).
[35] Y. Le Page and P. Saxe, Phys. Rev. B **65**, 104104 (2002).
[36] Z. Wu, E. Zhao, H. Xiang, X. Hao, X. Liu, and J. Meng, Phys. Rev. B **76**, 054115 (2007).
[37] F. Mouhat and F. X. Coudert, Phys. Rev. B **90**, 224104 (2014).
[38] A. Mujica, A. Rubio, A. Muñoz, and R. J. Needs, Rev. Mod. Phys. **75**, 863 (2003).
[39] R. G. Hennig, A. Wadehra, K. P. Driver, W. D. Parker, C. J. Umrigar, and J. W. Wilkins, Phys. Rev. B **82**, 014101 (2010).
[40] A. L. Wysocki, A. Kutepov, and V. P. Antropov, Phys. Rev. B **94**, 140405(R) (2016).